https://doi.org/10.5194/egusphere-2026-2795
Preprint. Discussion started: 1 July 2026

Emission control redirects aerosol formation toward nocturnal oxidant chemistry: Observations at a Korean petrochemical complex

Jaeuk Kim[1], Sungjin Park[1], Jihye Moon[1], Jaewon Seo[1], Jungho Yu[2], Seonjin Yoon[2], Jeungwoon Kim[2], and Hwajin Kim[1]

[1]Department of Environmental Health Science, Graduate School of Public Health, Seoul National University, Seoul, South Korea
[2]Institute of Health and Environmental Research, Chungcheongnam-do, 8 Hongyegongwon-ro, Hongvuk-eup, Hongseoung-gun, Chungcheongnam-do, 32254, Republic of Korea

Correspondence to: Hwajin Kim (khj0116@snu.ac.kr)

Abstract.

Industrial emission-control programs limit primary emissions to reduce aerosols, yet certain chemical and meteorological conditions can paradoxically enhance secondary formation. We report wintertime measurements of submicron aerosol composition at the Daesan Petrochemical Industrial Complex, South Korea (2023–2024), using a High-Resolution Time-of-Flight Aerosol Mass Spectrometer (HR-ToF-AMS) with trace-gas and meteorological data. Although mean aerosol concentrations were modest (14.9 ± 16.9 μg m^{-3}), episodic pollution was dominated by secondary species (86% of total mass). The atmosphere exhibited a titration-suppressed, oxidant-rich regime, with elevated ozone (30–40 ppb) maintained by reduced NO titration. This sustained nighttime oxidation via NO_3 and N_2O_5 chemistry, driving nitrate formation through heterogeneous hydrolysis and secondary organic aerosol (SOA) production after sunset. Comparable day–night correlations between Ox (= $O_3 + NO_2$) and the more-oxidized organic aerosol fraction ($r \approx 0.5$) indicate that nocturnal oxidation of industrial VOCs drives SOA formation. Meteorological stagnation amplified these processes: nitrate and MO-OOA were enhanced 6.6-fold and 3.1-fold relative to general conditions while O_3 rose only ~10%, demonstrating that the enhancement was driven by chemical conversion rather than accumulation, also supported by elevated ΔSOA/ΔCO ratios during stagnation. NOx-only emission control can therefore shift industrial atmospheres toward nocturnal, titration-suppressed regimes; effective mitigation requires coordinated management of reactive VOCs.

https://doi.org/10.5194/egusphere-2026-2795
Preprint. Discussion started: 1 July 2026

1 Introduction

Atmospheric aerosols, defined as stable suspensions of fine solid or liquid particles, play a pivotal role in air quality, human health, and the Earth's radiation balance. They scatter and absorb solar radiation, alter cloud properties, and serve as carriers of toxic substances (Pöschl, 2005; Zhang et al., 2015). In densely populated or industrialized regions, elevated concentrations of fine aerosols have been linked to severe haze events, reduced visibility, and substantial public-health burdens (Cohen et al., 2017; Guo et al., 2014; Huang et al., 2014). Aerosols originate both from direct (primary) emissions and from secondary processes involving the oxidation of gaseous precursors such as volatile organic compounds (VOCs), sulfur dioxide (SO_2), and nitrogen oxides (NO_x). Understanding how these primary and secondary pathways interact under different chemical regimes remains a central question in atmospheric chemistry.

Industrial complexes are among the most significant localized sources of air pollution due to the concentrated nature of manufacturing and petrochemical operations (Gao et al., 2021). These facilities emit a complex mixture of primary particles and reactive precursors that can lead to extensive secondary aerosol formation (Ding et al., 2025). Petrochemical plants, in particular, release large quantities of VOCs that participate in gas-phase oxidation and subsequent condensation to form secondary organic aerosol (SOA) (Bahreini et al., 2009; Li et al., 2021). However, most previous studies have examined the downwind influence of industrial emissions from urban or regional receptor sites (e.g., (Ju et al., 2020; Lee et al., 2025; Won et al., 2024)). Direct in-situ characterization within industrial zones remains scarce, limiting our understanding of the immediate atmospheric processing of fresh emissions and their transformation into secondary aerosols. A recent companion study at the Daesan Petrochemical Industrial Complex resolved seven distinct industrial VOC source factors (including catalyst production, plastics manufacturing, chlorinated chemical production, high-temperature pyrolysis, refinery operations, and terephthalic acid production) using on-site PTR-ToF-MS measurements (Hong et al., 2026), establishing that emissions in this complex are dominated by episodic, process-driven releases rather than diurnal or meteorological cycles. Notably, the terephthalic acid (TPA) production factor was identified as the dominant contributor to secondary organic aerosol formation potential despite representing only a minor fraction of total VOC mass (Hong et al., 2026). However, the corresponding aerosol-phase response, particularly how these reactive VOCs are coupled to oxidant chemistry and secondary aerosol formation under emission-controlled conditions, has not yet been directly observed.

In South Korea, the Daesan Petrochemical Industrial Complex represents one of the country's largest centers of industrial activity and the second-largest ethylene production base after Yeosu (Kim, 2022). To manage pollutant releases, continuous monitoring is conducted through the national Tele-Monitoring System (TMS), which tracks major primary pollutants such as PM, SO_2, NO_x, CO, and NH_3 in real time (Corporation, 2024). While this system has been effective in reducing directly emitted pollutants, it does not account for non-regulated precursors such as VOCs and semi-volatile organics, nor for the secondary products arising from their oxidation. As a result, the chemical behavior of aerosols and their dependence on oxidant chemistry and meteorological conditions remain poorly constrained in emission-controlled industrial regions.

https://doi.org/10.5194/egusphere-2026-2795
Preprint. Discussion started: 1 July 2026

This limitation leads to a critical bias: even where direct emissions are tightly regulated, substantial aerosol formation can continue, or even intensify, through secondary processes. Recent studies suggest that aggressive NO_x control may alter the atmospheric chemical regime by shifting from a photochemical-limited state to a titration-suppressed state, particularly at night (Kenagy et al., 2018; Ma et al., 2023). Under these conditions, the suppression of NO titration allows O_3 and NO_3 radicals to persist, acting as dominant oxidants. (Wang et al., 2023; Zhang et al., 2022). However, how these chemical regime shifts manifest in petrochemical complexes, where reactive VOC emissions remain abundant (Hong et al., 2026) and meteorological stagnation frequently occurs, remain poorly quantified. In particular, the coupling between emission control, oxidant redistribution, and meteorological confinement has yet to be examined using real-time, high-resolution observations within an active industrial complex.

To address this gap, we conducted the first high-resolution, real-time characterization of submicron aerosol composition within the Daesan Petrochemical Industrial Complex during winter 2023-2024. Measurements using a High-Resolution Time-of-Flight Aerosol Mass Spectrometer (HR-ToF-AMS), combined with gas-phase and meteorological observations, provide direct insight into the processes governing oxidant-driven secondary formation. By integrating chemical composition, source apportionment via Positive Matrix Factorization (PMF), and meteorological analysis, we aim: (1) characterize the composition and sources of aerosols; (2) elucidate the mechanisms linking NO_x reduction to oxidant redistribution, and (3) distinguish between physical accumulation and active chemical production during stagnation episodes using meteorological normalization. The results reveal a regime shift in industrial atmospheric chemistry, from a photochemistry-driven daytime state to a nocturnal, titration-suppressed state, where O_3 and NO_3 radicals govern both nitrate and SOA formation. These findings highlight the need to expand industrial air-quality management from primary-emission control toward integrated regulation of precursors, oxidants, and meteorological drivers of secondary aerosol formation.

2 Experimental methods

2.1 Sampling site description

Daesan, located in the western coastal region of South Korea, is a major industrial area facing the Yellow Sea (Fig. 1a). The region is the location of one of Korea's largest petrochemical complexes, emitting substantial amounts of air pollutants throughout the year. In this study, real-time measurements of particle chemical composition and size distributions were conducted at a site located within the Daesan Petrochemical Industrial Complex (37.01°N, 126.39°E). The sampling was conducted inside a container installed at the site, with the aerosol sampling inlet positioned at approximately 4 meters above ground level. The site is surrounded by dense industrial facilities and is adjacent to residential and agricultural areas within a few kilometers (Fig. 1b-c). Various emission sources and meteorological conditions during the measurement period were considered in the analysis.

https://doi.org/10.5194/egusphere-2026-2795
Preprint. Discussion started: 1 July 2026

2.2 Measurements

The NR-PM_1 chemical components, including organics, nitrate, ammonium, sulfate, and chloride, as well as their size distributions, were measured by an Aerodyne high-resolution time-of-flight aerosol mass spectrometer (HR-ToF-AMS) at a time resolution of 3 min. The HR-ToF-AMS was operated in both "V" and "W" modes, where high sensitivity with low mass resolution and low sensitivity with high mass resolution were achieved, respectively. Mass spectra (MS) and efficient particle time-of-flight (ePToF) data were acquired in standard configuration. Ionization efficiency (IE) and particle sizing calibrations were performed according to standard protocols (Canagaratna et al., 2007) before, during, and after the measurement period.

The black carbon (BC) concentration was measured using a multi-wavelength dual-spot Aethalometer (model AE33, Magee Scientific, Aerosol d.o.o.; Drinovec et al. (2015)), which continuously measures the attenuation of light transmitted through aerosol-laden filter spots at seven wavelengths. The dual-spot design corrects for loading artifacts by comparing a sample spot with a reference spot, improving the accuracy of long-term measurements.

Aerosol number size distributions in the mobility diameter range of 14.1 to 710.5 nm were measured using a scanning mobility particle sizer (SMPS 3080; TSI Inc., St Paul, MN, US). The SMPS classifies particles based on their electrical mobility using a differential mobility analyzer (DMA), followed by counting with a condensation particle counter (CPC). This setup enables high-resolution measurement of particle number concentrations as a function of size, which is essential for interpreting aerosol dynamics, aging, and growth processes. All the instruments sampled ambient air downstream of a $PM_{2.5}$ cyclone (URG Corp., Chapel Hill, NC, US), ensuring removal of coarse particles.

To characterize the precursors of secondary organic aerosols, volatile organic compounds (VOCs) were measured using a PTR-ToF-MS (Ionicon, Innsbruck, Austria) with a time resolution of 1 min. Key species including aromatics (benzene, toluene, ethylbenzene) and oxygenated VOCs were quantified. Detailed calibration procedures are provided in Hong et al. (2026).

Hourly concentrations of trace gases such as CO, O_3, NO_2, and SO_2 were obtained from the Korea Environment Corporation (K-eco) at the Dokgot-ri site (36.99°N, 126.38°E) (http://www.airkorea.or.kr). Although the station is located approximately 1 km from the aerosol sampling site, the terrain between the two points is flat with no significant intervening emission sources. Furthermore, the wind sector analysis (Fig. S6) confirms that both sites are influenced by the same industrial air masses, ensuring the representativeness of the gas-phase data. In addition, CO_2 concentration was measured using a non-dispersive infrared CO_2 analyzer (LI-850; LI-COR, Lincoln, NE, US) to serve as a tracer for anthropogenic activity and aid in interpreting aerosol and trace gas variability.

Meteorological data including ambient temperature, relative humidity (RH), wind speed, and wind direction were acquired from the nearby Daesan site (37.01°N, 126.39°E), operated by the Korea Meteorological Administration (http://www.kma.go.kr). The Daesan site is located approximately 800 m from the sampling site. All data are reported in local time, Korea Standard Time (KST), which is 9 hours ahead of Universal Coordinated Time (UTC).

https://doi.org/10.5194/egusphere-2026-2795
Preprint. Discussion started: 1 July 2026

2.3 AMS data analysis

2.3.1 Basic HR-ToF-AMS data analysis

HR-ToF-AMS data were processed and analyzed using the standard toolkit (SeQUential Igor data RetRiEval, SQUIRREL, ver. 1.66, and PIKA, ver. 1.26; available for download at (http://cires.colorado.edu/jimenez-group/ToFAMSResources/ToFSoftware/index.html) within Igor Pro 9 (WaveMatrics, Lake Oswego, OR, US). Details on the data processing procedures have been described in previous studies (Aiken et al., 2008; Aiken et al., 2009; Allan et al., 2004). Briefly, the standard fragmentation table described by (Allan et al., 2004) was used, with some small modifications to process the raw MS. The modifications were based on data from five filtered air measurements. This allowed measurements of the background from the gas-phase signal, which needed to be removed from the particle-phase measurement. Adjustments were made to the measured CO_2^+ (m/z = 44) signal to remove the contribution from gas-phase CO_2 as well as the $^{16}O^+$-to-$^{14}N^+$ ratio for air signals at m/z = 29 based on measurements of particle-free ambient air.

Relative ionization efficiencies (RIE) of 1.1, 1.11, and 3.19 were used for nitrate, sulfate, and ammonium, respectively, based on values determined from calibration using pure NH_4NO_3 and $(NH_4)_2SO_4$ aerosols. A composition-dependent collection efficiency (CE) was applied to the data based on an algorithm by Middlebrook et al. (2012). Nitrate was observed to be an important component of NR-PM_1 during this study (31%), although the campaign average (±1σ) CE was 0.5 ± 0.06. The size distribution calibration was conducted during the campaign using the standard polystyrene latex (PSL) spheres (90, 150, 220, 300, 400, 450, 500, 600, 800 nm) following the standard AMS procedures (Canagaratna et al., 2007).

The mass-based size distributions measured by AMS were consistent with volume-based size distributions from SMPS measurements throughout the campaign. Detection limits for major AMS species are summarized in Table S1. All AMS mass concentrations reported in this study are based on ambient temperature and pressure.

The elemental ratios between oxygen, carbon, hydrogen, nitrogen, and sulfur, as well as the organic mass-to-carbon ratio (OM/OC) of OA, were determined from an analysis of the W-mode high resolution mass spectra (HRMS) data, following the method reported by Canagaratna et al. (2015). Unless otherwise indicated, the O/C, H/C, and OM/OC ratios stated in this paper from other studies have been calculated using the updated elemental analysis method (Canagaratna et al., 2015).

2.3.2 Positive matrix factorization (PMF) analysis

The HRMS data of organic aerosol were analyzed using positive matrix factorization (PMF). The analysis was conducted using the PMF2 algorithm in robust mode (Paatero & Tapper, 1994), with the PMF Evaluation Toolkit (PET ver. 3.06A) (Ulbrich et al., 2009). Data and error matrices were prepared following the protocols of Ulbrich et al. (2009) and Zhang et al. (2011). Briefly, a minimum error value was applied, ions with signal-to-noise ratio (SNR) < 0.2 were removed, and those with 0.2 < SNR < 2 were downweighted by a factor of 2. Ions associated with m/z 44 (CO_2^+, CO^+, H_2O^+, HO^+, and O^+) were also downweighted to prevent overestimation. After these treatments, the final matrix contained 243 ions (m/z 12-120).

https://doi.org/10.5194/egusphere-2026-2795
Preprint. Discussion started: 1 July 2026

PMF solutions with one to nine factors were explored, and the appropriate number of factors was determined based on Q/Q_{exp}, mass spectral features, diurnal variations, and correlations with external tracers following (Zhang et al., 2011) (Fig. S1). Rotational ambiguity was assessed by varying the fPeak parameter from −1 to +1 in increments of 0.2. The four-factor solution (fPeak = 0, Q/Q_{exp} = 1.34) was selected because it provided a stable and physically interpretable separation of OA sources. The three-factor solution failed to separate traffic- and solid-fuel-related components, while the five-factor solution yielded redundant factors with similar O/C and N/C ratios, suggesting over-splitting of sources (Fig. S2). Therefore, the four-factor solution was judged to best represent distinct OA types in Daesan during winter.

As a result, four OA factors were identified hydrocarbon-like OA (HOA), solid fuel OA (SFOA), and two oxygenated OA components, less oxidized OOA (LO-OOA) and more oxidized OOA (MO-OOA) (Fig. 2 and Sect. S1). HOA was characterized by hydrocarbon fragment ions (e.g., m/z 41, 43, 55, 57), representing vehicular and industrial combustion emissions. SFOA exhibited strong signals at m/z 60, 73 and also contained PAH-related fragments and alkyl ions, indicating primary emissions from solid fuel combustion in the region. LO-OOA (O/C = 0.53, H/C = 1.65) showed partial compositional overlap with SFOA (m/z 60, 73) but exhibited a more oxidized spectrum, indicating that it represents a less-aged, early-stage oxidized OA derived from SFOA-related emissions. This interpretation is reinforced by significant correlations with combustion-related VOCs, including chlorobenzene (C_6H_5Cl, r = 0.63), which can originate from waste incineration, and naphthalene ($C_{10}H_8$, r = 0.61), a PAH consistent with solid-fuel aerosol signatures (Fig.S10c) (Hsu et al., 2021; Jiang et al., 2023). Together, these relationships suggest that LO-OOA reflects partially oxidized SFOA rather than newly formed VOC-driven secondary OA. MO-OOA (O/C = 1.03, H/C = 1.28) represented aged, highly oxidized OA formed under stagnant atmospheric conditions. Overall, secondary OA (LO-OOA + MO-OOA) accounted for ~63% of total OA mass, whereas primary OA (HOA + SFOA) contributed 37%, indicating that both primary solid-fuel emissions and secondary formation processes were important sources of OA in Daesan during winter.

2.4 Back-trajectory analysis

In this study, 72h back trajectories were calculated every hour using version 5.2.1 of the Hybrid Single-Particle Lagrangian Integrated Trajectory (HYSPLIT) model (Draxler, 2025) for the sampling periods from 8 December 2023 to 16 January 2024. The trajectories were released at half of the mixing height at the Daesan Petrochemical Complex (latitude: 37.00°N, longitude: 126.39°E) and the average arriving height for the back trajectories for this study was approximately 430 m. To identify the pollutant characteristics in different predominant transport patterns, cluster analysis was performed on the trajectory using the software HYSPLIT5 and four clustered trajectories were identified according to their similarity in a spatial distribution. Individual back trajectories in each cluster are shown in Fig. S7.

https://doi.org/10.5194/egusphere-2026-2795
Preprint. Discussion started: 1 July 2026

3 Results and discussion

3.1 Wintertime Aerosol Characteristics in the Daesan Petrochemical Complex

During the winter campaign (8 December 2023-16 January 2024), PM_1 concentrations in Daesan exhibited large temporal variability, ranging from 0.4 to 141.9 μg m^{-3} with an average of 14.9 ± 16.9 μg m^{-3} (Fig. 3). Although mean levels were moderate compared with typical urban winter values, distinct high-loading episodes occurred under specific meteorological conditions, indicating that secondary processes and stagnation episodes can offset emission-control benefits. Assuming PM_1 accounts for approximately 80% of $PM_{2.5}$, about 10% of sampling days exceeded the Korean daily $PM_{2.5}$ standard (35 μg m^{-3}).

The average chemical composition of PM_1+BC was dominated by organic aerosol (32.2%) and nitrate (31.2%), followed by ammonium (15.9%), sulfate (13.3%), black carbon (5.1%), and chloride (2.3%) (Fig. S3a). Within the OA fraction, secondary organic aerosol (SOA = LO-OOA + MO-OOA) contributed 63% while primary OA (HOA + SFOA) comprised 37%. Notably, solid fuel OA (SFOA) accounted for 21% of OA. Given the industrial setting and the strong correlation with chloride (r = 0.73) and industrial VOC tracers (Fig. S9, S10e-f), this factor is likely linked to industrial waste incineration or solid-fuel boilers within the complex, rather than residential wood burning (S1). This highlights that primary industrial emissions remain non-negligible, yet secondary processes (NO_3^- + SO_4^{2-} + NH_4^+ + SOA) accounted for ≈ 83% of the PM_1+BC mass) clearly dominate. Temporal patterns of nitrate, OA, and meteorological parameters (Fig. 3) reveal that high-PM_1+BC events correspond to calm wind conditions and shallow mixing layers. The relatively high nitrate fraction and moderate sulfate contribution suggest that oxidation of local NOx and VOC precursors, rather than long-range sulfate transport, was the dominant driver of secondary particle mass. These results establish the basis for subsequent analysis of the oxidation regime and formation mechanisms (Sects. 3.2-3.4).

3.2 Shift from Photochemical to Nocturnal Oxidant Chemistry

In typical wintertime urban atmospheres, nitrate formation proceeds primarily through daytime photochemical oxidation of NO_2 to HNO_3 and subsequent partitioning to aerosol NH_4NO_3 (Yang et al., 2022). However, Daesan exhibits a distinct "titration-suppressed regime". In this study, we use "titration-suppressed regime" to denote a NO_x-controlled atmospheric state in which the reduction of NO emissions weakens the O_3 + NO titration sink, leading to elevated nocturnal O_3 and sustained NO_3/N_2O_5 production. We note that this terminology refers to nocturnal radical chemistry and is distinct from the photochemical "NO_x-limited" or "VOC-limited" ozone production regimes defined for daytime tropospheric chemistry. Throughout the remainder of this paper, "titration-suppressed regime" is used consistently to denote this nocturnal state, and "oxidant-driven" is used only as a descriptor for chemistry or formation pathways that proceed through O_3, NO_3, or N_2O_5. As shown in Fig. 4a, O_3 generally exceeded NO_2 throughout the campaign, with data clustering above the 1:1 line and within the NO_2-limited regime, distinct from the O_3-limited conditions commonly observed in high-NO_x cities. On average, O_3

https://doi.org/10.5194/egusphere-2026-2795
Preprint. Discussion started: 1 July 2026

concentrations reached 33.7 ppb while NO_2 remained below 13.1 ppb, reflecting suppressed NO titration and enhanced oxidant persistence.

Although N_2O_5 and NO_3 radicals were not directly measured, their nighttime chemistry can be inferred from co-variations of O_3 and NO_2. The formation of NO_3 follows $O_3 + NO_2 \rightarrow NO_3 + O_2$, and N_2O_5 accumulates through $NO_3 + NO_2 \rightleftharpoons N_2O_5$. Hence, the product $[O_3][NO_2]$ represents a first-order proxy for potential NO_3/N_2O_5 formation, while the NO_2/O_3 ratio governs whether the chemistry is limited by O_3 or NO_2. In Daesan, the frequent dominance of O_3 ($NO_2/O_3 < 1$) indicates that N_2O_5 formation was throttled by NO_2 scarcity rather than by lack of O_3 (Ma et al., 2023). When NO_2/O_3 approached unity in the pre-dawn, nitrate concentrations rose sharply (Fig. 4b-c), especially under relative humidity exceeding 70% (Fig. S4). The strong NO_3^- correlation with RH and O_x thus is consistent with heterogeneous N_2O_5 hydrolysis as a major nocturnal nitrate pathway, alongside potential contributions from gas–particle partitioning of HNO_3 formed during the day (Figs. S4a and 5a). This preservation of O_3 is a direct consequence of strict NO_x emission controls. With insufficient NO to titrate ozone, the production of NO_3 radicals ($NO_2 + O_3 \rightarrow NO_3$) can proceed efficiently. Theoretical estimation of the NO_3 production rate, $p(NO_3) = k[NO_2][O_3]$, indicates sustained radical generation throughout the night (Fig. 4). Here, the temperature-dependent rate coefficient k(T) for the $NO_2 + O_3$ reaction was taken from Atkinson et al. (2004) as $k(T) = 1.4 \times 10^{-13} \exp(-2470/T)$ cm^3 $molecule^{-1}$ s^{-1}, evaluated at the observed nighttime T. To express $p(NO_3)$ in molecule cm^{-3} s^{-1}, the measured NO_2 and O_3 mixing ratios (ppb) were converted to number densities using the ideal-gas law at the observed T and P. The resulting $p(NO_3)$ time series (Fig. 4) confirms that NO_3 radical production proceeds continuously through the night at rates comparable to those reported for other NO_x-rich environments. In addition, particulate nitrate accumulation was examined as a function of the dry aerosol surface area density (S_a) integrated from SMPS size distributions (~14–700 nm). Under high-RH (>70%) conditions, exhibited a positive dependence on Sa (Fig. S4b), qualitatively consistent with heterogeneous reactive uptake on particle surfaces. When the data are further stratified by RH, the slope of NO3⁻ versus [O3][NO2] under RH ≥ 70% was approximately twice that under RH < 70% (Fig. S4a), supporting the role of aqueous-phase chemistry. We note that S_a here is the dry-state value and is expected to underestimate the in-situ wet surface area at high RH by a factor of ~1.3–1.5; this caveat reinforces, but does not alter, the qualitative trend.

Diurnal profiles confirm this interpretation: nitrate and ammonium increased steadily from 19:00 to 01:00 LT and again from 04:00 to 08:00, then declined rapidly after sunrise, coinciding with boundary-layer growth and temperature increase (Figs. 4b-d and S5). This pattern reflects volatilization and dilution rather than photochemical production. The nighttime buildup contrasts sharply with Seoul and Beijing winter campaigns, where higher NOx and stronger photochemistry produce daytime nitrate maxima (Duan et al., 2020; Kim et al., 2017). In Daesan's low-NO_x environment, oxidation capacity persisted despite reduced photochemical activity, maintained instead by O_3-driven nocturnal chemistry.

To quantify this regime behavior, the relationship between nitrate concentration and the NO_2/O_3 ratio was examined during the pre-dawn period (02:00–07:00 LT), prior to sunrise and before the onset of daytime boundary-layer development. During this period, nitrate concentrations closely tracked variations in the NO_2/O_3 ratio, exhibiting a strong correspondence that

https://doi.org/10.5194/egusphere-2026-2795
Preprint. Discussion started: 1 July 2026

supports the presence of a NO_2-limited regime in Daesan. Notably, nitrate concentrations increased markedly as the NO_2/O_3 ratio approached unity.

When the dataset was separated by relative humidity, the slope of NO_3^- versus $[O_3][NO_2]$ under RH $\geq$ 70% was approximately twice that observed under RH < 70%, accompanied by a stronger correlation (Fig. S4a). This behavior indicates that nitrate formation via heterogeneous uptake and hydrolysis of N_2O_5 was substantially enhanced under high-humidity conditions. Collectively, these results demonstrate that, despite the NO_2-limited regime, Daesan can sustain efficient nighttime oxidation when sufficient humidity and aerosol surface area are available (Fig. S4b).

Mechanistically, this contrasts with O_3-limited (high-NO_x) conditions, where NO titration suppresses O_3 and thereby inhibits NO_3 radical formation. In such environments, daytime OH + NO_2 dominates total nitrate yield, and nocturnal pathways are minor. In Daesan's NOx-controlled, titration-suppressed atmosphere, reduced NO titration maintains high O_3, sustaining continuous production of NO_3 radicals and promoting N_2O_5 hydrolysis throughout the night. Consequently, nitrate formation becomes oxidant-limited rather than photochemical-limited, reflecting a shift from a daytime to a nocturnal oxidant regime.

In summary, even without direct N_2O_5 measurement, the O_3-NO_2 phase-space analysis and diurnal nitrate behavior together indicate that Daesan's wintertime aerosol chemistry is governed by NO_2-limited, oxidant-driven nocturnal formation. This redistribution of oxidation capacity under emission control establishes the mechanistic basis for the coupled nitrate-SOA enhancement discussed in Sect. 3.3.

3.3 Coupled Formation of Nitrate and Secondary Organic Aerosol

The redistributed oxidation capacity also governed organic aerosol (OA) evolution. Despite weak daytime photochemistry, the oxygenated fraction of OA (OOA = LO-OOA + MO-OOA) remained persistently high throughout the campaign, averaging 63% of total OA and 21% of total PM_1+BC (Fig. S3a). This abundance of oxidized organics in a low-NOx, emission-controlled environment indicates that the same nocturnal oxidants responsible for nitrate formation also sustained dark secondary organic aerosol (SOA) production. As shown in Fig. 5b, the fractional contribution of more-oxidized OOA (MO-OOA) correlated strongly with the total oxidant concentration ($Ox = O_3 + NO_2$) with comparable correlation coefficients during day ($r = 0.52$) and night ($r = 0.53$). The similarity of these day-night relationships indicates that oxidant-driven SOA formation proceeds with comparable efficiency in both periods at Daesan, with nocturnal chemistry contributing substantially to total SOA mass rather than acting as a secondary process. Sustained nighttime oxidation is supported by elevated O_3 and persistent NO_3 radicals. Hence, oxidant availability, rather than photochemical intensity, was the dominant control on organic aerosol evolution.

Co-located VOC measurements provided mechanistic insight (Fig. 6). A companion VOC study at the same site (Hong et al., 2026) used PTR-ToF-MS measurements and Positive Matrix Factorization to resolve seven major industrial source factors at Daesan and showed that, although the terephthalic acid (TPA) production factor accounted for only ~3% of total VOC mass, it contributed ~32% of the total SOA formation potential, the largest among all resolved sources. The TPA factor, marked by

https://doi.org/10.5194/egusphere-2026-2795
Preprint. Discussion started: 1 July 2026

benzaldehyde and C8 aromatics, was persistently emitted throughout the campaign, including at night. To assess the potential role of these industrial VOCs as nighttime SOA precursors, we examined the relationships between MO-OOA and two representative species, benzaldehyde and ethylbenzene, using binned boxplots (Fig. 6). MO-OOA concentrations increased systematically with rising benzaldehyde and ethylbenzene levels, demonstrating a positive relationship between precursor availability and oxidized aerosol production. Similar to MO-OOA, the polar distribution patterns of both VOCs indicate that they originated primarily from local emission sources rather than long-range transport.

These nocturnal emissions, occurring when O_3 concentrations remained high (> 30 ppb) and NO_2 was low (< 15 ppb), provided a reactive substrate for NO_3-initiated oxidation and ozonolysis. Because the NO_2/O_3 ratio (< 1 most nights) favored NO_3 formation and hindered titration, freshly emitted VOCs could undergo rapid dark oxidation, yielding multifunctional low-volatility products that condensed into particles. The predominance of MO-OOA with O/C ≈ 1.0 (Fig. 2) is consistent with such multiphase processing. This interpretation is supported by the VOC–OA relationships shown in Fig. 6: nighttime increases in benzaldehyde and ethylbenzene were systematically followed by enhancements in MO-OOA, indicating that freshly emitted VOCs served as efficient nighttime SOA precursors. Because these relationships were derived exclusively from nocturnal measurements (19:00–07:00 LT), they reflect dark-oxidation processes rather than photochemistry.

Comparisons of Ox and MO-OOA, as well as Ox and particulate nitrate during nighttime, further demonstrate the contribution of nocturnal oxidation, with production sensitivities of 0.6, 0.9, and 4.1 μg m^{-3} per 10 ppb for MO-OOA and 1.0, 0.9, and 9.6 μg m^{-3} per 10 ppb for nitrate across the 30-40, 40-50, and 50-60 ppb Ox intervals (Fig. 5c-d). Importantly, these enhancements were not accompanied by proportional increases in primary tracers. As shown in Fig. 7, black carbon (BC) concentrations declined systematically with increasing mixing-layer height, and the highest SOA/OA ratios (> 0.7) occurred when MLH < 1000 m. This relationship indicates that the nighttime accumulation of oxidized OA was linked primarily to boundary-layer confinement and secondary formation, rather than to direct primary emissions. The absence of co-variation with CO or BC therefore supports a local, secondary origin of the observed SOA.

Periods of low mixing-layer height (≈ 388 m) and high humidity amplified these processes by enhancing gas-particle partitioning and aqueous-phase reactions, increasing SOA mass fractions by 18% relative to well-mixed conditions (Fig. 8). Such stagnant, humid nights effectively turned the industrial basin into a dark, oxidant-rich reactor consistent with the titration-suppressed regime defined in Sect. 3.2, where irregular nocturnal precursor emissions and persistent oxidants sustained coupled production of nitrate and SOA. Collectively, these results indicate that in Daesan's NOx-controlled environment, photochemistry is no longer the principal driver of secondary formation: persistent O_3 and NO_3 radicals, together with nighttime VOC emissions, maintain a locally driven oxidant-SOA formation regime, setting the stage for the meteorological amplification discussed in Sect. 3.4.

3.4 Meteorological Amplification of Oxidant-Driven Secondary Formation

Although the Daesan complex operates under strict emission control, several high-concentration episodes occurred during the campaign, indicating that meteorology played a decisive role in amplifying oxidant-driven secondary formation (Fig. 8 and

https://doi.org/10.5194/egusphere-2026-2795
Preprint. Discussion started: 1 July 2026

Table 1). Four such episodes ($PM_1 > 28$ μg m^{-3}) were identified on December 24, 27, 29, and January 5, each coinciding with low wind speeds (≈ 2.5 m s^{-1}), shallow boundary layers (≈ 388 m), and high relative humidity (≈ 77%) (Table 1). These conditions satisfy the stagnation criteria of (Gao et al., 2020) and represent an atmosphere highly susceptible to accumulation and multiphase processing. Back-trajectory analysis (Fig. S7) showed that the air masses during these events (Cluster 2) originated from low-altitude transport (< 1 km AGL) over eastern China and the Yellow Sea before decelerating above the complex. The combination of regional recirculation, weak vertical mixing, and persistent high humidity produced an ideal environment for secondary aerosol buildup.

During these stagnant periods, the concentrations of both primary and secondary species increased, but the enhancement was far greater for the latter. Relative to general conditions, nitrate increased by approximately 6.6×, LO-OOA by 6.9×, and MO-OOA by 3.1×, whereas O_3 rose only modestly (~ 10%) (Fig. 8 and Table 1). Such disproportionate increases in condensed-phase species compared to gaseous oxidants demonstrate that the high loading did not arise from intensified photochemistry, but from efficient multiphase conversion and particle growth under confined meteorological conditions. Particle-size distributions (Fig. S8) shifted toward larger accumulation-mode diameters (≈ 470-620 nm), consistent with condensational growth and aqueous-phase reactions. The high relative humidity promoted N_2O_5 hydrolysis and organic uptake, while low boundary-layer turbulence allowed these processes to proceed without dilution. Together, these factors produced sharp nighttime rises in nitrate and MO-OOA that persisted until the following morning's vertical mixing.

The stagnation also influenced the local chemical regime itself. When the mixing layer collapsed, surface O_3 accumulated and NO_2/O_3 ratios approached unity, further enhancing nocturnal NO_3 and N_2O_5 formation (Fig. 4 and Sect. 3.2). Simultaneously, relative humidity close to 80% increased aerosol liquid water content, favoring heterogeneous uptake and aqueous-phase oxidation. As a result, the chemical lifetime of VOCs shortened, but their product yield to the particle phase increased. This feedback loop, low dispersion, high humidity, elevated oxidants, and locally emitted precursors, created an environment where both nitrate and SOA formation were self-reinforcing.

Meteorological amplification was most evident on December 24, 27, 29, and January 5, when persistent surface inversions trapped emissions overnight. The resulting PM_1 buildup reached a peak of 141.9 μg m^{-3}, with nitrate and MO-OOA accounting for more than 47% of total mass (Fig. 8). Daytime dissipation of the boundary layer temporarily reduced concentrations through dilution and volatilization, but mass rapidly re-accumulated the following evening as conditions re-stagnated. These diurnal cycles confirm that the variability in aerosol concentrations was controlled primarily by boundary-layer dynamics rather than emission fluctuations. Nighttime VOC emissions, which persisted throughout the period (Sect. 3.3), further intensified these episodes by supplying precursors precisely when oxidant chemistry and humidity favored secondary production (Hong et al., 2026).

Overall, the results demonstrate that meteorological confinement acts as a powerful amplifier of oxidant-driven chemistry in an emission-controlled industrial environment. Stagnant, humid nights foster N_2O_5 hydrolysis and NO_3-initiated oxidation, enabling continuous formation of nitrate and SOA even under reduced NOx levels. The synergy between chemical regime

https://doi.org/10.5194/egusphere-2026-2795
Preprint. Discussion started: 1 July 2026

shifts and meteorological stagnation thus explains why Daesan experiences episodic pollution peaks despite low average PM_1+BC concentrations.

3.5 Scope and limitations

Several limitations of this study should be acknowledged when interpreting the proposed mechanisms. First, the inferred role of nocturnal N_2O_5 hydrolysis is based on the $[NO_2][O_3]$ production proxy and the observed dependence of nitrate accumulation on aerosol surface area and relative humidity; direct measurements of NO_3 radical, N_2O_5, and $ClNO_2$ together with explicit quantification of the effective N_2O_5 uptake coefficient remain important targets for future work. Second, NH_3 and HNO_3 were not measured during the campaign, which precludes a full thermodynamic analysis of HNO_3/particulate-NO_3^- partitioning. We therefore cannot rule out a contribution of daytime HNO_3 formation followed by nocturnal repartitioning to the particle phase to the observed nitrate accumulation; the relative weight of in-situ N_2O_5 chemistry versus partitioning warrants further investigation with collocated gas-phase measurements and thermodynamic modeling (e.g., ISORROPIA-II with measured NH_3/HNO_3). Third, attribution of nocturnal SOA to industrial VOCs draws on the companion study of Hong et al. (2026); the present observations establish only an association between MO-OOA and benzaldehyde/ethylbenzene, not a causal source assignment. Fourth, the inferred regime characteristics are derived from a single five-week winter campaign at one site, and seasonal and inter-annual variability remain to be tested. Despite these limitations, the dataset represents one of the first detailed in-situ characterizations of submicron aerosols within an active, emission-controlled petrochemical complex, and the qualitative regime shift identified here should be testable by future, more instrumented campaigns.

4 Conclusions and implications

The Daesan observations reveal the emergence of a chemically distinct atmospheric regime within a heavily regulated petrochemical complex. Despite substantial reductions in primary and nitrogen-oxide emissions, wintertime air quality remained dominated by secondary aerosol formation. The results indicate a transition from a photochemistry-driven daytime state to a nocturnal, titration-suppressed system (as defined in Sect. 3.2), in which O_3 and NO_3 radicals, not OH, serve as the principal oxidants controlling both nitrate and secondary organic aerosol (SOA) production. Under this regime, oxidation and particle growth persist long after sunset through heterogeneous N_2O_5 hydrolysis and dark oxidation of locally emitted volatile organic compounds (VOCs).

This regime shift arises as a consequence of effective emission controls. Reducing NOx lowers photochemical activity and daytime HNO_3 formation but simultaneously elevates O_3 by weakening titration, thereby enhancing nighttime oxidant chemistry. The interplay of high O_3, low NO_2, and abundant reactive VOCs enables continuous production of NO_3 radicals, which oxidize unsaturated and aromatic hydrocarbons to form highly oxygenated organic nitrates and other low-volatility species. The co-variation of nitrate and oxygenated OA, supported by their shared dependence on oxidant concentration and

https://doi.org/10.5194/egusphere-2026-2795
Preprint. Discussion started: 1 July 2026

relative humidity, indicates that the aerosol population in Daesan is sustained by oxidant redistribution rather than photochemical intensity.

Meteorological confinement further amplifies these processes. Stagnant boundary layers, low wind speeds, and high humidity suppress dilution and promote multiphase reactions, extending the lifetime of oxidants and precursors. During such episodes, nitrate increased by up to sixfold and MO-OOA by up to threefold relative to background conditions, while O_3 changed only slightly. The resulting environment functions as a dark oxidation reactor, a confined, humid, oxidant-rich atmosphere where secondary aerosol production continues efficiently even under reduced emissions. These findings carry four implications for atmospheric chemistry and air-quality management. (1) Re-evaluation of NO_x-only emission control strategies. Policies emphasizing NO_x reduction alone may inadvertently enhance nocturnal oxidant chemistry and secondary aerosol formation in industrial regions where reactive VOCs remain abundant; mitigation should include coordinated control of VOC precursors and continuous monitoring of oxidant species. (2) Inclusion of nocturnal NO_3/N_2O_5 chemistry in air-quality models. Chemical-transport and air-quality models should explicitly represent N_2O_5 uptake, dark SOA pathways, and their sensitivity to humidity and boundary-layer dynamics to predict PM responses under emission-control scenarios. (3) Recognition of industrial complexes as nocturnal atmospheric reactors. The coexistence of high VOC emissions and reduced NO_x creates oxidizing environments that sustain secondary production at night; such sites can serve as natural laboratories for evaluating coupled nitrate–SOA formation in future studies. (4) Chemistry–meteorology coupling in air-quality forecasting. The strong dependence of oxidant-driven aerosol formation on stagnation highlights the need to integrate meteorological forecasting (boundary-layer height, ventilation) with chemical predictions: stable boundary layers not only trap pollutants but also accelerate their chemical transformation.

In summary, the Daesan case exemplifies how industrial regions under emission control can evolve into oxidant-enhanced, nocturnal chemical systems where secondary formation persists, or intensifies, despite low average PM levels. Effective mitigation will require a shift from species-specific regulation toward a process-oriented framework that couples emission reduction with precursor management, oxidant monitoring, and meteorological forecasting. This paradigm is essential for achieving genuine improvements in air quality within next-generation emission-controlled industrial environments.

Data availability. The hourly ambient temperature, RH, WS and WD data were acquired from the Korea Meteorological Administration (http://www.kma.go.kr). The hourly trace gas data (e.g., CO, SO_2, O3 and NO_2 concentrations) were acquired from the Korea Environment Corporation (K eco) (http://www.airkorea.or.kr). The other observational data used in this study are available from the corresponding author upon reasonable request.

Author contributions.

Conceptualization, Methodology, Writing—review & editing, H.K.; Methodology, Investigation, Analysis, Writing—original draft, J. K..; Field measurements and data acquisition —S. P. and J. M.; Field support— J. Y., S. Y. and J. K.

https://doi.org/10.5194/egusphere-2026-2795
Preprint. Discussion started: 1 July 2026

Declaration of competing interests

The authors declare that they have no known competing financial interests or personal relationships that could have appeared to influence the work reported in this paper.

Acknowledgements.

This work was supported by the National Research Foundation of Korea (NRF) grant funded by the Korea government (MSIT) (RS-2025-00514570). Also this work is supported by the Seoul National University (SNU) Creative-Pioneering Program for Young Researchers **:** 'Development of SMaRT-based aerosol measurement and analysis systems for the evaluation of climate change and health risk assessment'.(900-20250086).

References

Aiken, A. C., DeCarlo, P. F., Kroll, J. H., Worsnop, D. R., Huffman, J. A., Docherty, K. S., Ulbrich, I. M., Mohr, C., Kimmel, J. R., Sueper, D., Sun, Y., Zhang, Q., Trimborn, A., Northway, M., Ziemann, P. J., Canagaratna, M. R., Onasch, T. B., Alfarra, M. R., Prevot, A. S. H.,…Jimenez, J. L. (2008). O/C and OM/OC Ratios of Primary, Secondary, and Ambient Organic Aerosols with High-Resolution Time-of-Flight Aerosol Mass Spectrometry. *Environmental Science & Technology*, *42*(12), 4478-4485. https://doi.org/10.1021/es703009q

Aiken, A. C., Salcedo, D., Cubison, M. J., Huffman, J. A., DeCarlo, P. F., Ulbrich, I. M., Docherty, K. S., Sueper, D., Kimmel, J. R., Worsnop, D. R., Trimborn, A., Northway, M., Stone, E. A., Schauer, J. J., Volkamer, R. M., Fortner, E., de Foy, B., Wang, J., Laskin, A.,…Jimenez, J. L. (2009). Mexico City aerosol analysis during MILAGRO using high resolution aerosol mass spectrometry at the urban supersite (T0) – Part 1: Fine particle composition and organic source apportionment. *Atmos. Chem. Phys.*, *9*(17), 6633-6653. https://doi.org/10.5194/acp-9-6633-2009

Allan, J. D., Delia, A. E., Coe, H., Bower, K. N., Alfarra, M. R., Jimenez, J. L., Middlebrook, A. M., Drewnick, F., Onasch, T. B., Canagaratna, M. R., Jayne, J. T., & Worsnop, D. R. (2004). A generalised method for the extraction of chemically resolved mass spectra from Aerodyne aerosol mass spectrometer data. *Journal of Aerosol Science*, *35*(7), 909-922. https://doi.org/https://doi.org/10.1016/j.jaerosci.2004.02.007

Bahreini, R., Ervens, B., Middlebrook, A. M., Warneke, C., de Gouw, J. A., DeCarlo, P. F., Jimenez, J. L., Brock, C. A., Neuman, J. A., Ryerson, T. B., Stark, H., Atlas, E., Brioude, J., Fried, A., Holloway, J. S., Peischl, J., Richter, D., Walega, J., Weibring, P.,…Fehsenfeld, F. C. (2009). Organic aerosol formation in urban and industrial plumes near Houston and Dallas, Texas. *Journal of Geophysical Research: Atmospheres*, *114*(D7). https://doi.org/https://doi.org/10.1029/2008JD011493

Canagaratna, M. R., Jayne, J. T., Jimenez, J. L., Allan, J. D., Alfarra, M. R., Zhang, Q., Onasch, T. B., Drewnick, F., Coe, H., Middlebrook, A., Delia, A., Williams, L. R., Trimborn, A. M., Northway, M. J., DeCarlo, P. F., Kolb, C. E., Davidovits, P., & Worsnop, D. R. (2007). Chemical and microphysical characterization of ambient aerosols with the aerodyne aerosol mass spectrometer. *Mass Spectrometry Reviews*, *26*(2), 185-222. https://doi.org/https://doi.org/10.1002/mas.20115

Canagaratna, M. R., Jimenez, J. L., Kroll, J. H., Chen, Q., Kessler, S. H., Massoli, P., Hildebrandt Ruiz, L., Fortner, E., Williams, L. R., Wilson, K. R., Surratt, J. D., Donahue, N. M., Jayne, J. T., & Worsnop, D. R. (2015). Elemental ratio measurements of organic compounds using aerosol mass spectrometry: characterization, improved calibration, and implications. *Atmos. Chem. Phys.*, *15*(1), 253-272. https://doi.org/10.5194/acp-15-253-2015

Cohen, A. J., Brauer, M., Burnett, R., Anderson, H. R., Frostad, J., Estep, K., Balakrishnan, K., Brunekreef, B., Dandona, L., Dandona, R., Feigin, V., Freedman, G., Hubbell, B., Jobling, A., Kan, H., Knibbs, L., Liu, Y., Martin, R., Morawska, L.,…Forouzanfar, M. H. (2017). Estimates and 25-year trends of the global burden of disease attributable to ambient

https://doi.org/10.5194/egusphere-2026-2795
Preprint. Discussion started: 1 July 2026

air pollution: an analysis of data from the Global Burden of Diseases Study 2015. *The Lancet*, *389*(10082), 1907-1918. https://doi.org/https://doi.org/10.1016/S0140-6736(17)30505-6

Corporation, M. o. E. a. K. E. (2024). *굴뚝 원격감시체계 업무편람*. https://dl.nanet.go.kr/SearchDetailView.do?cn=MONO12025000017952&sysid=nadl

Ding, Z., Li, Y., Fu, Q., Tian, M., Wang, F., Wang, Y., & Huang, K. (2025). Volatile organic compounds in a typical petrochemical production area in Shanghai, China: Source profiles, human health and environmental impacts. *Environmental Pollution*, *372*, 126074. https://doi.org/https://doi.org/10.1016/j.envpol.2025.126074

Draxler, R., Stunder, B., Rolph, G., Stein, A., Taylor, A., Zinn, S., Loughner, C., and Crawford, A. (2025). *HYSPLIT User's Guide*. NOAA Air Resources Laboratory. https://www.arl.noaa.gov/documents/reports/hysplit_user_guide.pdf

Drinovec, L., Močnik, G., Zotter, P., Prévôt, A. S. H., Ruckstuhl, C., Coz, E., Rupakheti, M., Sciare, J., Müller, T., Wiedensohler, A., & Hansen, A. D. A. (2015). The "dual-spot" Aethalometer: an improved measurement of aerosol black carbon with real-time loading compensation. *Atmos. Meas. Tech.*, *8*(5), 1965-1979. https://doi.org/10.5194/amt-8-1965-2015

Duan, J., Huang, R. J., Li, Y., Chen, Q., Zheng, Y., Chen, Y., Lin, C., Ni, H., Wang, M., Ovadnevaite, J., Ceburnis, D., Chen, C., Worsnop, D. R., Hoffmann, T., O'Dowd, C., & Cao, J. (2020). Summertime and wintertime atmospheric processes of secondary aerosol in Beijing. *Atmos. Chem. Phys.*, *20*(6), 3793-3807. https://doi.org/10.5194/acp-20-3793-2020

Gao, G., Wang, S., Xue, R., Liu, D., Ren, H., & Zhang, R. (2021). Uncovering the characteristics of air pollutants emission in industrial parks and analyzing emission reduction potential: case studies in Henan, China. *Scientific Reports*, *11*(1), 23709. https://doi.org/10.1038/s41598-021-03193-z

Gao, Y., Zhang, L., Zhang, G., Yan, F., Zhang, S., Sheng, L., Li, J., Wang, M., Wu, S., Fu, J. S., Yao, X., & Gao, H. (2020). The climate impact on atmospheric stagnation and capability of stagnation indices in elucidating the haze events over North China Plain and Northeast China. *Chemosphere*, *258*, 127335. https://doi.org/https://doi.org/10.1016/j.chemosphere.2020.127335

Guo, S., Hu, M., Zamora, M. L., Peng, J., Shang, D., Zheng, J., Du, Z., Wu, Z., Shao, M., Zeng, L., Molina, M. J., & Zhang, R. (2014). Elucidating severe urban haze formation in China. *Proceedings of the National Academy of Sciences*, *111*(49), 17373-17378. https://doi.org/doi:10.1073/pnas.1419604111

Hsu, Y.-C., Chang, S.-H., & Chang, M. B. (2021). Emissions of PAHs, PCDD/Fs, dl-PCBs, chlorophenols and chlorobenzenes from municipal waste incinerator cofiring industrial waste. *Chemosphere*, *280*, 130645. https://doi.org/https://doi.org/10.1016/j.chemosphere.2021.130645

Hong, S.-I., Park, S., Kim, J., Park, S., Moon, J., de Gouw, J., Yu, J., Yoon, S., Kim, J., & Kim, H. (2026). Episodic and source-resolved VOC emissions in a petrochemical complex: Insights from real-time measurements. *Environmental Pollution*, *397*, 128032. https://doi.org/10.1016/j.envpol.2026.128032

Huang, R.-J., Zhang, Y., Bozzetti, C., Ho, K.-F., Cao, J.-J., Han, Y., Daellenbach, K. R., Slowik, J. G., Platt, S. M., Canonaco, F., Zotter, P., Wolf, R., Pieber, S. M., Bruns, E. A., Crippa, M., Ciarelli, G., Piazzalunga, A., Schwikowski, M., Abbaszade, G.,…Prévôt, A. S. H. (2014). High secondary aerosol contribution to particulate pollution during haze events in China. *Nature*, *514*(7521), 218-222. https://doi.org/10.1038/nature13774

Jiang, W., Peng, Y., Tang, M., Xiong, S., Chen, K., Lu, S., & Wang, F. (2023). PCDD/Fs emissions in a large-scale hazardous waste incinerator under different operation conditions: Effective reduction strategies and an applicable correlation. *Journal of the Energy Institute*, *107*, 101186. https://doi.org/https://doi.org/10.1016/j.joei.2023.101186

Ju, S., Yu, G. H., Park, S., Lee, J. Y., Lee, S., Jee, J., Lee, K., & Lee, M. (2020). Pollution Characteristics of PM2.5 Measured during Fall at a Seosan Site in Chungcheong Province. *Journal of Korean Society for Atmospheric Environment*, *36*(3), 329-345. https://doi.org/10.5572/KOSAE.2020.36.3.329

Kenagy, H. S., Sparks, T. L., Ebben, C. J., Wooldrige, P. J., Lopez-Hilfiker, F. D., Lee, B. H., Thornton, J. A., McDuffie, E. E., Fibiger, D. L., Brown, S. S., Montzka, D. D., Weinheimer, A. J., Schroder, J. C., Campuzano-Jost, P., Day, D. A., Jimenez, J. L., Dibb, J. E., Campos, T., Shah, V.,…Cohen, R. C. (2018). NOx Lifetime and NOy Partitioning During WINTER. *Journal of Geophysical Research: Atmospheres*, *123*(17), 9813-9827. https://doi.org/https://doi.org/10.1029/2018JD028736

Kim, H., Zhang, Q., Bae, G. N., Kim, J. Y., & Lee, S. B. (2017). Sources and atmospheric processing of winter aerosols in Seoul, Korea: insights from real-time measurements using a high-resolution aerosol mass spectrometer. *Atmos. Chem. Phys.*, *17*(3), 2009-2033. https://doi.org/10.5194/acp-17-2009-2017

https://doi.org/10.5194/egusphere-2026-2795
Preprint. Discussion started: 1 July 2026

Kim, Y.-J. a. K., Young-Soo. (2022). *Daesan Petrochemical Industrial Complex (Daesan Coastal Industrial Area): Conversion Plan to a National Industrial Complex*. https://www.cni.re.kr/main/contents/report/view.do?docId=1022JU009

Lee, S.-J., Lee, H.-Y., Kim, S.-J., Kim, S.-H., Noh, S., & Choi, S.-D. (2025). Pollution characteristics and cancer risk of PAHs in a petrochemical industrial city: Insights from passive air sampling and three-dimensional dispersion modeling. *Journal of Hazardous Materials*, *500*, 140423. https://doi.org/https://doi.org/10.1016/j.jhazmat.2025.140423

Li, K., Wentzell, J. J., Liu, Q., Leithead, A., Moussa, S. G., Wheeler, M. J., Han, C., Lee, P., Li, S.-M., & Liggio, J. (2021). Evolution of atmospheric total organic carbon from petrochemical mixtures. *Environmental Science & Technology*, *55*(19), 12841-12851.

Ma, P., Quan, J., Dou, Y., Pan, Y., Liao, Z., Cheng, Z., Jia, X., Wang, Q., Zhan, J., Ma, W., Zheng, F., Wang, Y., Zhang, Y., Hua, C., Yan, C., Kulmala, M., Liu, Y., Huang, X., Yuan, B.,…Liu, Y. (2023). Regime-Dependence of Nocturnal Nitrate Formation via N2O5 Hydrolysis and Its Implication for Mitigating Nitrate Pollution. *Geophysical Research Letters*, *50*(24), e2023GL106183. https://doi.org/https://doi.org/10.1029/2023GL106183

Middlebrook, A. M., Roya, B., L., J. J., & and Canagaratna, M. R. (2012). Evaluation of Composition-Dependent Collection Efficiencies for the Aerodyne Aerosol Mass Spectrometer using Field Data. *Aerosol Science and Technology*, *46*(3), 258-271. https://doi.org/10.1080/02786826.2011.620041

Paatero, P., & Tapper, U. (1994). Positive matrix factorization: A non-negative factor model with optimal utilization of error estimates of data values. *Environmetrics*, *5*(2), 111-126. https://doi.org/https://doi.org/10.1002/env.3170050203

Pöschl, U. (2005). Atmospheric Aerosols: Composition, Transformation, Climate and Health Effects. *Angewandte Chemie International Edition*, *44*(46), 7520-7540. https://doi.org/https://doi.org/10.1002/anie.200501122

Ulbrich, I. M., Canagaratna, M. R., Zhang, Q., Worsnop, D. R., & Jimenez, J. L. (2009). Interpretation of organic components from Positive Matrix Factorization of aerosol mass spectrometric data. *Atmos. Chem. Phys.*, *9*(9), 2891-2918. https://doi.org/10.5194/acp-9-2891-2009

Wang, H., Wang, H., Lu, X., Lu, K., Zhang, L., Tham, Y. J., Shi, Z., Aikin, K., Fan, S., Brown, S. S., & Zhang, Y. (2023). Increased night-time oxidation over China despite widespread decrease across the globe. *Nature Geoscience*, *16*(3), 217-223. https://doi.org/10.1038/s41561-022-01122-x

Won, S. R., Lee, K., Song, M., Kim, C., Jang, K.-S., & Lee, J. Y. (2024). Characteristic of PM2.5 concentration and source apportionment during winter in Seosan, Korea. *Asian Journal of Atmospheric Environment*, *18*(1), 22. https://doi.org/10.1007/s44273-024-00044-x

Yang, S., Yuan, B., Peng, Y., Huang, S., Chen, W., Hu, W., Pei, C., Zhou, J., Parrish, D. D., Wang, W., He, X., Cheng, C., Li, X. B., Yang, X., Song, Y., Wang, H., Qi, J., Wang, B., Wang, C.,…Shao, M. (2022). The formation and mitigation of nitrate pollution: comparison between urban and suburban environments. *Atmos. Chem. Phys.*, *22*(7), 4539-4556. https://doi.org/10.5194/acp-22-4539-2022

Zhang, Q., Jimenez, J. L., Canagaratna, M. R., Ulbrich, I. M., Ng, N. L., Worsnop, D. R., & Sun, Y. (2011). Understanding atmospheric organic aerosols via factor analysis of aerosol mass spectrometry: a review. *Analytical and Bioanalytical Chemistry*, *401*(10), 3045-3067. https://doi.org/10.1007/s00216-011-5355-y

Zhang, R., Wang, G., Guo, S., Zamora, M. L., Ying, Q., Lin, Y., Wang, W., Hu, M., & Wang, Y. (2015). Formation of Urban Fine Particulate Matter. *Chemical Reviews*, *115*(10), 3803-3855. https://doi.org/10.1021/acs.chemrev.5b00067

Zhang, Y.-L., Zhang, W., Fan, M.-Y., Li, J., Fang, H., Cao, F., Lin, Y.-C., Wilkins, B. P., Liu, X., Bao, M., Hong, Y., & Michalski, G. (2022). A diurnal story of Δ17O($$\rm{NO}_{3}^{-}$$) in urban Nanjing and its implication for nitrate aerosol formation. *npj Climate and Atmospheric Science*, *5*(1), 50. https://doi.org/10.1038/s41612-022-00273-3

https://doi.org/10.5194/egusphere-2026-2795
Preprint. Discussion started: 1 July 2026

555

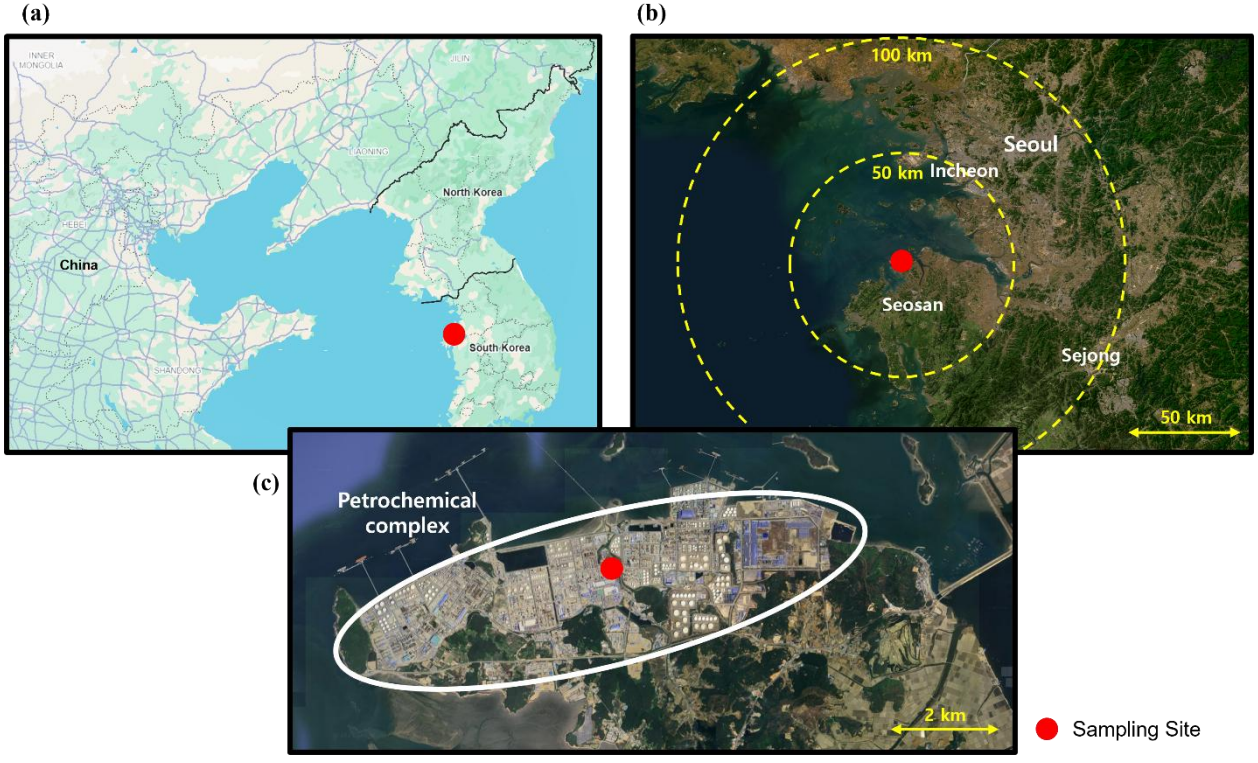

560 **Figure 1 (a) A map of Korea showing its location next to China. (b) Location of the sampling site within the country. (c) Location of the sampling site and the Daesan petrochemical industrial complex around the sampling site. Satellite imagery and map data in Figure 1: Google Maps; imagery ©2026 Airbus, CNES / Airbus, Maxar Technologies; map data ©2026 Google.**

https://doi.org/10.5194/egusphere-2026-2795
Preprint. Discussion started: 1 July 2026

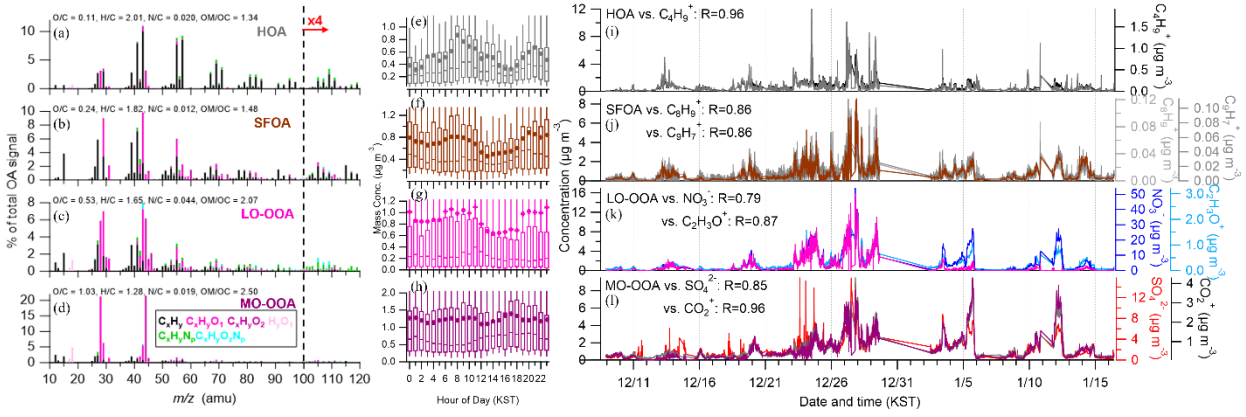

Figure 2 Overview of the results from PMF analysis, including high-resolution mass spectra of the (a) hydrocarbon-like organic aerosol (HOA), (b) solid fuel OA (SFOA), (c) low oxidized oxygenated OA (LO-OOA), and (d) more oxidized oxygenated OA (MO-OOA) colored by different ion families. (e-h) Average diurnal profiles of each of the OA factors (the 90th and 10th percentiles and denoted by the whiskers above and below the boxes. The 75th and 25th percentiles are denoted by the top and bottom of the boxes. The median values are denoted by the horizontal line within the box, and the mean values are denoted by the colored markers). (i-l) time series of the total organic aerosol (OA) of the four factors derived from the positive matrix factorization (PMF) analysis.

https://doi.org/10.5194/egusphere-2026-2795
Preprint. Discussion started: 1 July 2026

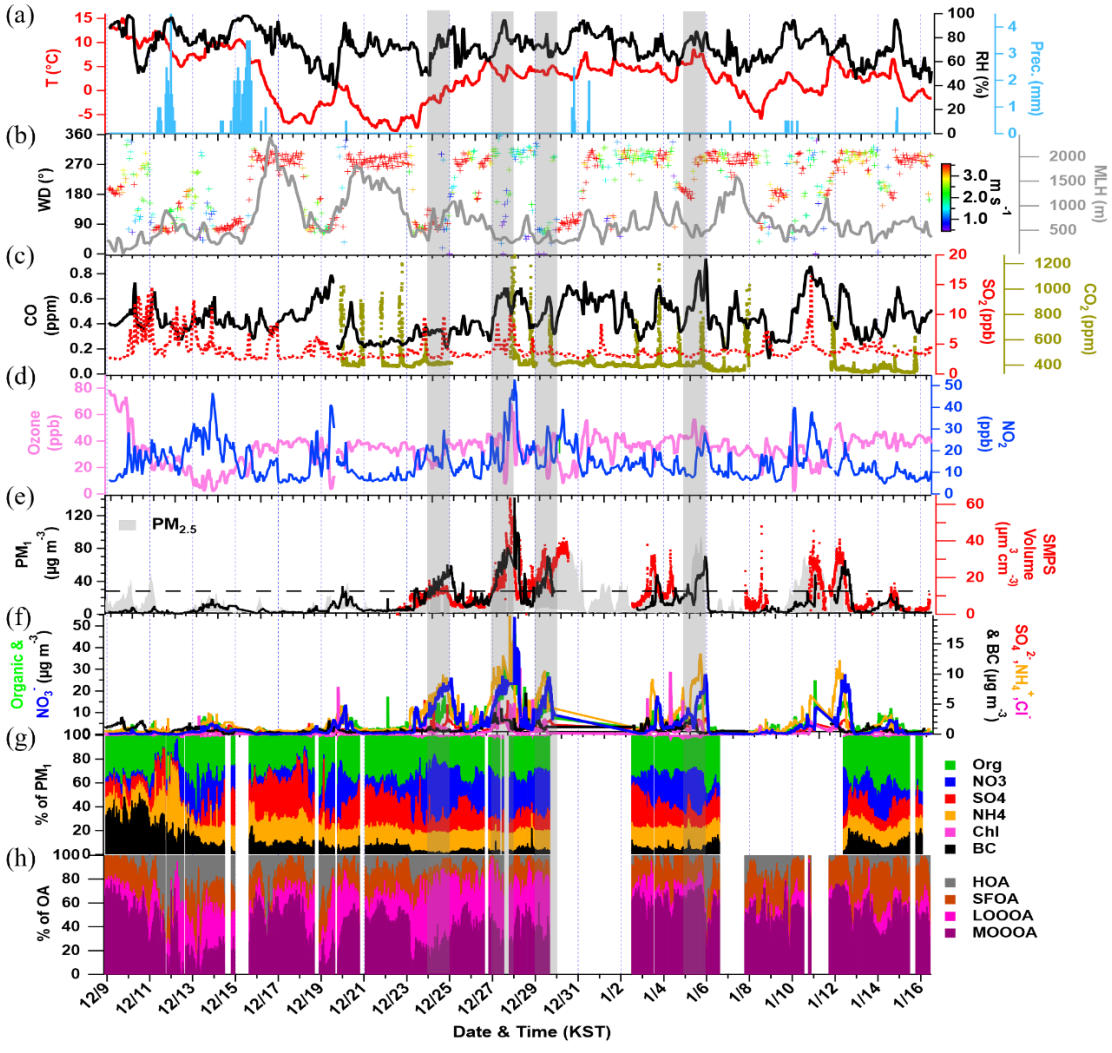

Figure 3 Overview of the temporal variations in submicron aerosols at the Daesan petrochemical industrial complex from 8 December 2023 to 16 January 2024. (a) Time series of ambient air temperature (T), relative humidity (RH), and precipitation (Prec.); (b) time series of wind direction (WD), with colors showing different wind speeds (WS); (c) time series of CO, SO_2, and CO_2; (d) time series of O_3 and NO_2; (e) time series of total particulate matter (PM_1), and scanning mobility particle sizer (SMPS) volume concentrations. Also shown are $PM_{2.5}$ from AirKorea as gray shading, daily PM_1 standard (28 μg m^{-3}) indicated by black dashed line; (f) time series of the organic aerosols, nitrate(NO_3^-), sulfate (SO_4^{2-}), ammonium (NH_4^+), chloride (Cl^-), and BC; (g) Time series of the mass fractional contribution of organic aerosols (Org), nitrate (NO3), sulfate (SO4), ammonium (NH4), chloride (Chl), and BC to total PM_1+BC; (h) time series of the mass fractional contribution to total organic aerosol (OA) of the four factors derived from the positive matrix factorization (PMF) analysis.

https://doi.org/10.5194/egusphere-2026-2795
Preprint. Discussion started: 1 July 2026

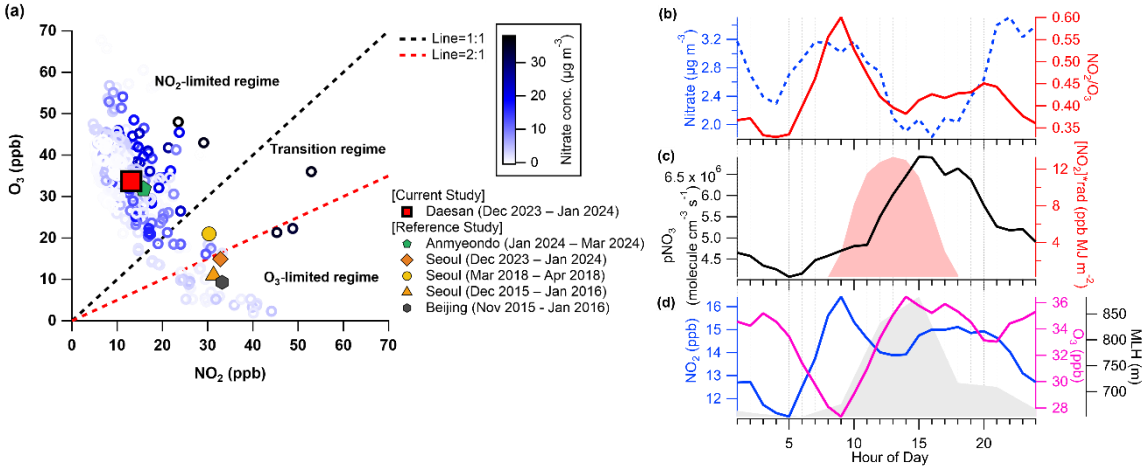

Figure 4 (a) Classification of nocturnal N_2O_5 formation regimes using the NO_2/O_3 ratio. According to Ma et al. (2023), efficient N_2O_5 production occurs when NO_2/O_3 ranges from 1 to 2. Nighttime observations at the Daesan site fall mostly within the NO_2-limited regime. The dashed lines indicate NO_2/O_3 = 1 (black) and 2 (red). (b) Temporal variations in NO_2/O_3 and nitrate concentrations from 01:00 to 07:00, a period minimally affected by MLH, highlighting the chemical production under NO_2-limited conditions. (c) Estimated N_2O_5 concentrations derived from NO_3 production calculated from NO_2 and O_3, along with the influence of solar radiation on oxidation. (d) Diurnal variations in NO_2, O_3, and MLH. Daytime decreases are primarily driven by MLH-induced dilution rather than photochemical production.

https://doi.org/10.5194/egusphere-2026-2795
Preprint. Discussion started: 1 July 2026

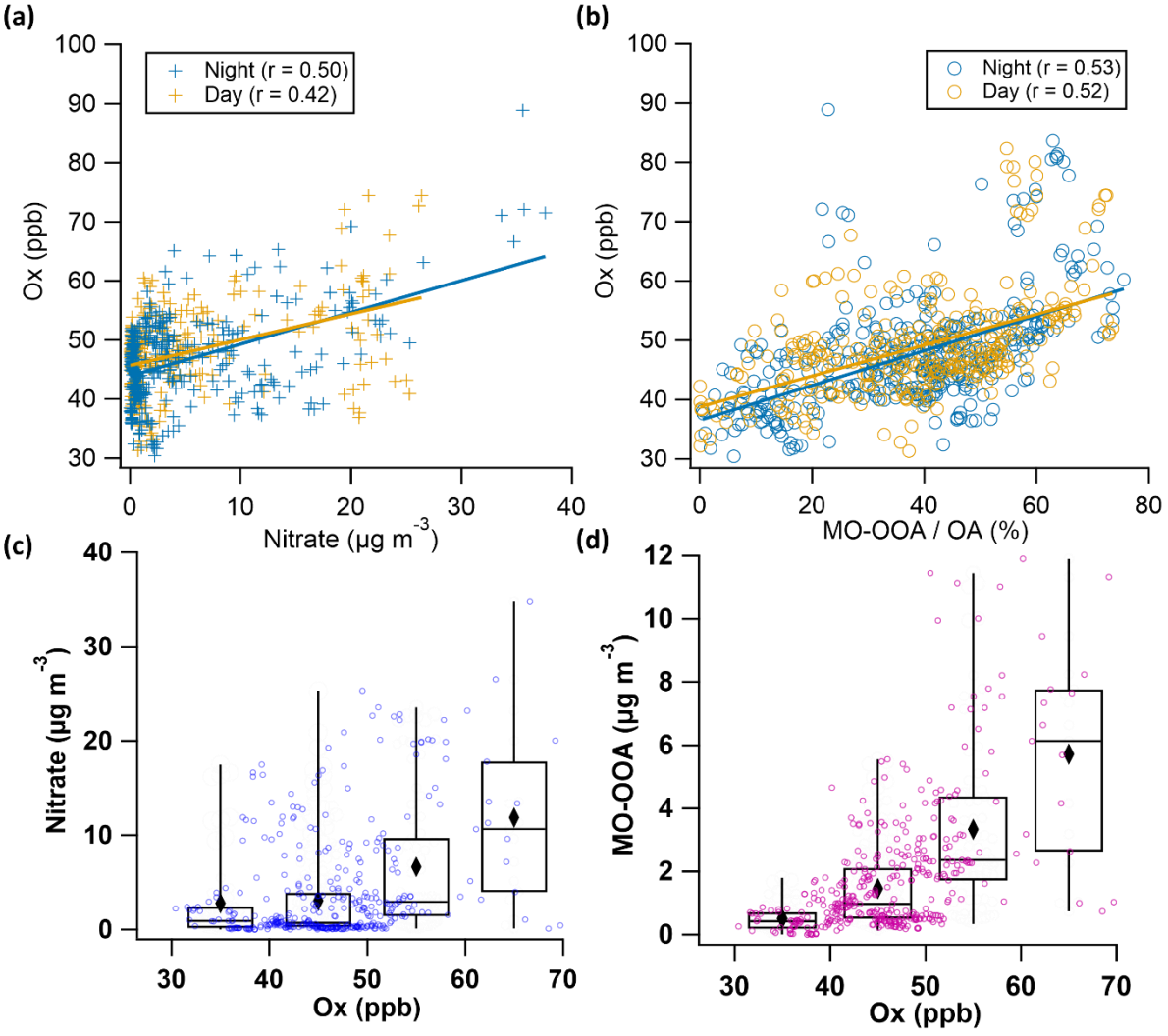

Figure 5 (a-b) Correlations of Ox with nitrate and MO-OOA/OA for daytime and nighttime periods. Comparable day–night correlations indicate that oxidant-driven secondary formation proceeded with similar efficiency in both periods at the Daesan site. (c-d) Increases in nitrate and MO-OOA with Ox, suggesting that both species are influenced by O_3-driven oxidation under NO_2-limited conditions. Only nighttime observations (19:00-07:00 LT) were used in this analysis. The boxplots show the median (central line), interquartile range (25th–75th percentiles, box), and the 10th–90th percentile whiskers; the diamond markers represent the mean values.

https://doi.org/10.5194/egusphere-2026-2795
Preprint. Discussion started: 1 July 2026

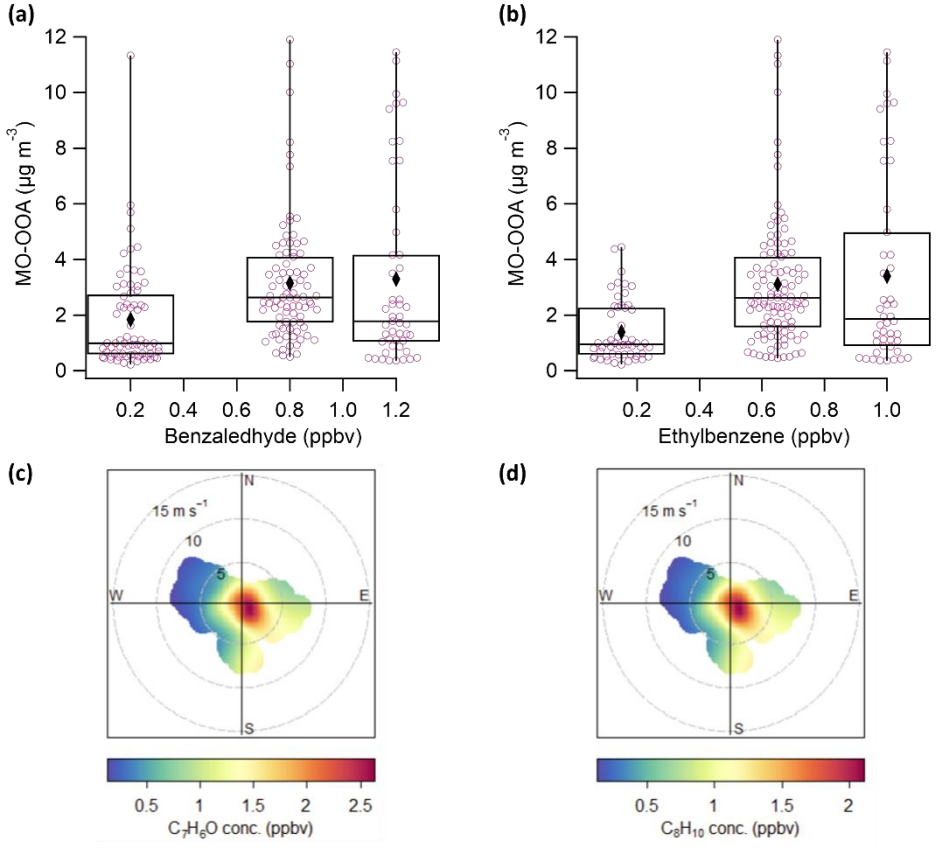

600 **Figure 6 (a–b) Boxplots showing the nighttime relationships between benzaldehyde (C_7H_6O) and ethylbenzene (C_8H_{10}) with MO-OOA concentrations under binned VOC levels. The boxplots indicate the median (central line), interquartile range (25th–75th percentiles, box), and the 10th–90th percentile whiskers; the diamond symbols represent the mean values. (c–d) Polar plots illustrating the wind dependence of benzaldehyde and ethylbenzene, respectively, with color shading indicating VOC concentrations as a function of wind speed and direction.**

605

https://doi.org/10.5194/egusphere-2026-2795
Preprint. Discussion started: 1 July 2026

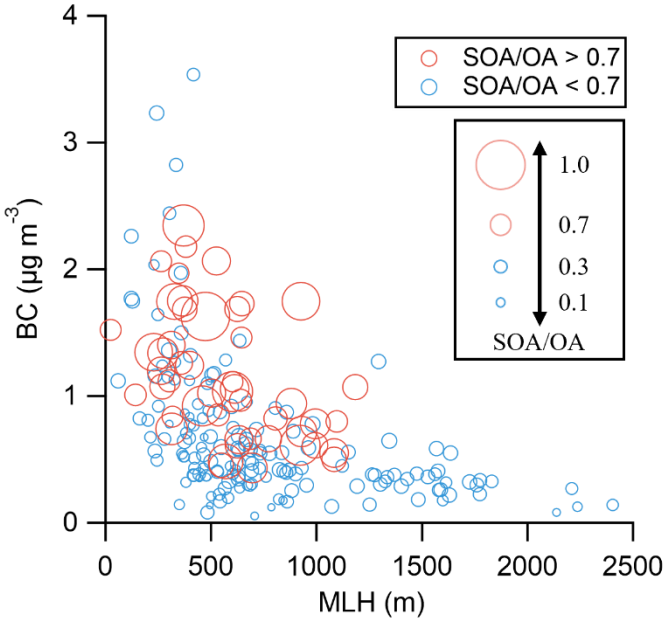

Figure 7 Relationship between BC and MLH, showing increased BC concentrations under shallow MLH due to accumulation. Red circles represent data with SOA/OA > 0.7, and blue circles represent SOA/OA<0.7; circle sizes indicate the SOA fraction. Enhanced SOA formation is observed under low-MLH conditions, where accumulation is pronounced.

610

https://doi.org/10.5194/egusphere-2026-2795
Preprint. Discussion started: 1 July 2026

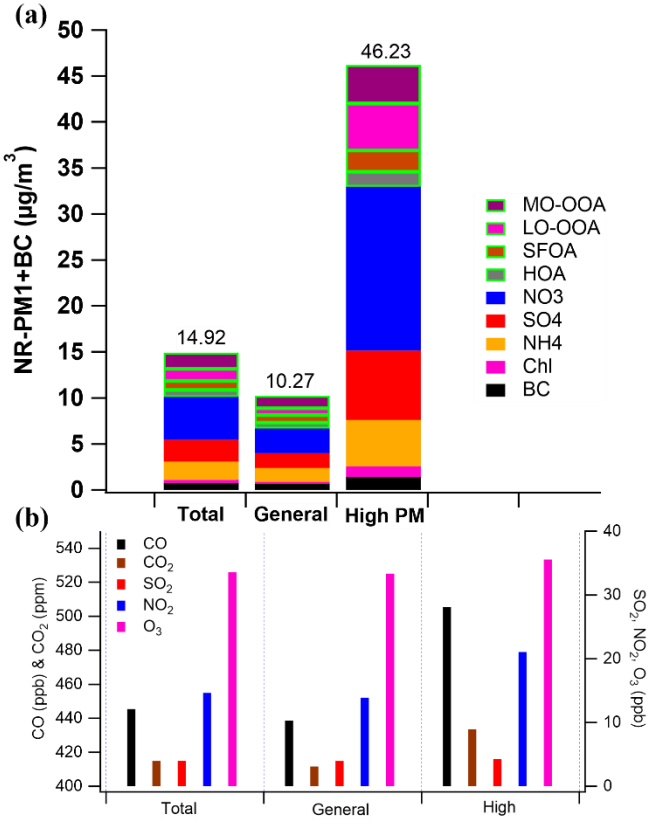

Figure 8 (a) Comparison of PM_1+BC chemical composition during the total period, the general period (non-high-PM), and the high-PM period ($PM_1 \geq 28$ μg m^{-3}). (b) Corresponding gas-phase species for the same three periods. Detailed numerical values are summarized in Table 1.

615

https://doi.org/10.5194/egusphere-2026-2795
Preprint. Discussion started: 1 July 2026

Table 1. Summary of aerosol composition, trace gases, and meteorological conditions during general and high-concentration periods.

(a) NR-PM$_1$ Composition (μg m^{-3})

Species	Total	General	High	H/G
MO-OOA	1.74	1.37	4.19	3.06
LO-OOA	1.31	0.74	5.11	6.93
SFOA	1.01	0.82	2.31	2.82
HOA	0.76	0.63	1.63	2.59
Nitrate	4.65	2.69	17.85	6.64
Sulfate	2.37	1.60	7.53	4.69
Ammonium	1.99	1.53	5.05	3.30
Chloride	0.34	0.22	1.14	5.09
BC	0.76	0.66	1.41	2.14
SUM	14.92	10.27	46.23	

(b) Trace Gases (ppb unless noted)

Species	Total	General	High	H/G
CO (ppb)	446	439	505	1.15
SO_2	3.99	3.96	4.27	1.08
NO_2	14.6	13.9	21.1	1.52
O_3	33.6	33.4	35.6	1.07
CO_2 (ppm)	415	412	434	1.05

(c) Meteorological and Regime Indicators

Variable	High conc.	General
PM (μg m^{-3})	**46.23**	10.27
RH (%)	**77**	72
WS (m/s)	2.5	**3.7**
MLH (m)	450	**723**
NO_2 (ppb)	**21.1**	13.9
CO (ppb)	**505.4**	438.5
NO_2/CO	**0.0417**	0.0317
Nitrate (μg m^{-3})	**17.83**	2.75